

EFFECT OF ELECTRIC PULSE TREATMENT ON MICROSTRUCTURE, ELECTROCHEMICAL AND DISCHARGE PROPERTIES OF AZ61 ANODES FOR Mg-AIR BATTERIESJinchao Zou^{a,b,*}, Tao Zhang^{a,b}, Zhiquan Huang^{a,b}, Chunjiang Zhao^{a,b,*} and Junpeng Wang^{a,b}^aHeavy Machinery Engineering Research Center of the Ministry of Education, Taiyuan University of Science and Technology, 030024 Taiyuan, China^bSchool of Mechanical Engineering, Taiyuan University of Science and Technology, 030024 Taiyuan, China

Recebido em 10/07/2022; aceito em 05/10/2022; publicado na web 12/01/2023

In this work, the effects of electric pulse treatment on the discharge and electrochemical properties of rolled and extruded AZ61 as anode of Mg-air battery were studied. The microstructure, electrochemical behavior and surface morphology after discharge were discussed to relate the discharge performance. The experimental results show that compared with the original magnesium anode (rolled and extruded), the magnesium anode treated by electric pulse has more negative corrosion potential, lower impedance value, higher discharge voltage and better specific energy. This is because electric pulse treatment can cause the coarse second phase in magnesium anode to dissolve and the grains to become more uniform. In particular, in the discharge process, the surface of magnesium anode after electric pulse treatment will form micro cracks, which is beneficial to promote the self-stripping of discharge products. It is worth noting that the effect of electric pulse treatment on rolled anode is better than that of extruded anode. It may be due to the different dislocation density in the two anodes. During the electric pulse treatment, the dislocation density in the alloy is highly correlated with the dissolution rate of β -Mg₁₇Al₁₂, which ultimately affects the volume fraction of the second phase in the alloy.

Keywords: Mg-air battery; electric pulse treatment; electrochemical performance; β -Mg₁₇Al₁₂; discharge properties.

INTRODUCTION

As fossil fuels and global warming continue to intensify worldwide, metal-air batteries have attracted wide attention due to their high energy density, low cost, high safety and environmental friendliness.^{1,2} Metal-air battery is a compact and inexpensive fuel cell. As one of the cathode reactants, oxygen in the air reduces the total weight of the battery, releases more energy storage space, and thus significantly improves the energy density.³⁻⁵ Among the currently used metal air battery series, Mg-air battery has been extensively studied due to its light weight, high negative electrode potential (-2.37 V vs. SHE), high theoretical energy density (6.8 kWh kg⁻¹) and excellent ecological friendliness.⁶⁻⁸

However, like other metal-air batteries, Mg-air batteries also have various technical problems, resulting in performance failing to meet theoretical expectations. For example, magnesium anode has relatively serious self-corrosion in electrolyte (especially in chloride solution), which greatly reduces the capacity of Mg-air battery.⁹ In addition, during the discharge process, due to the negative differential effect (NDE) and the insoluble Mg(OH)₂ discharge product coated on the surface of the magnesium anode, the discharge process is hindered, and the service life and performance of the battery are significantly reduced.¹⁰

In recent years, various methods have been developed to solve the existing problems in Mg-air batteries, and heat treatment has been proved to be one of the most effective methods.^{11,12} It is reported that heat treatment can effectively remove (MgZn)₃Gd eutectic phase in Mg-Gd-Zn magnesium anode, resulting in long period stacking order (LPSO) structure, which provides moderate and even stimulation for the dissolution of the α -Mg and helps to exfoliate the discharge products, greatly enhancing its discharge performance.¹³ Cao *et al.*¹⁴ found that Mg₃Gd alloy after solution treatment will dissolve Gd-containing particles which lead to serious galvanic corrosion,

significantly reducing the corrosion rate of Mg₃Gd, thereby improving the electrochemical properties of magnesium alloys. Studies have shown that heat treatment can change the microstructure and second phase distribution of ZK60 magnesium alloy, thereby affecting its self-corrosion behavior and electrochemical behavior.¹⁵ According to Ma *et al.*¹⁶ heat treatment can greatly increase the content of magnesium oxide on the corrosion surface of Mg-5Al-1Zn-1Sn magnesium alloy, thus separating the magnesium matrix from the corrosion electrolyte, reducing the corrosion rate of the alloy and improving the electrochemical performance of the alloy. In addition, Wang *et al.*¹⁷ showed that solid solution treatment could promote most small Mg₂Cu particles of Mg-Cu-Al magnesium alloy to dissolve in α -Mg, reduce the weight loss rate, and improve the corrosion resistance of the alloy. However, heat treatment has the problems of complex process, long process and high energy consumption.¹⁸ Therefore, it is urgent to find a simple process, short process and low energy consumption treatment method to improve the electrochemical and discharge performance of magnesium alloy.

With the in-depth study of electro plasticity by researchers, electric pulse treatment (EPT) has the characteristics of short-term efficiency and high energy, and has been gradually applied in metal processing as a new material processing method.^{19,20} Electrical pulse treatment refers to improving the microstructure of metal alloys by applying pulse current during or before deformation. In general, the properties of magnesium anodes are mainly determined by their chemical composition and microstructure characteristics.^{21,22} Therefore, electric pulse treatment can be used to improve the discharge properties of magnesium alloys. At present, most studies have focused on the effects of EPT on phase transformation,^{23,24} recrystallization²⁵ and mechanical properties.^{26,27} However, few studies have focused on the effects of EPT on the discharge properties of magnesium anode. Therefore, this work selected two different plastic deformation AZ61 magnesium alloy: rolled state and extruded state, in order to investigate the effect of EPT on the discharge properties of AZ61 magnesium anode with different plastic deformation under

*e-mail: zhaohj75@163.com

the same pulse parameter. At the same time, the corrosion behavior of the battery was also studied to facilitate the connection between the microstructure and the performance of the battery. In addition, in this work, four different alloys were assembled into Mg-air cells and tested at different current densities (2.5 mA cm⁻², 5 mA cm⁻², 10 mA cm⁻² and 20 mA cm⁻²), and the discharge performance was analyzed in detail. The purpose of this study is to explore the mechanism of EPT on the discharge properties of different magnesium anodes (rolled and extruded), and provide new ideas for the fabrication of magnesium anodes.

EXPERIMENTAL

Preparation of materials

The ingot and extruded AZ61 magnesium alloy sheet were provided by the manufacturer (Hebi Maitu Technology Co., LTD.), and the components of the samples were identified as 5.96% Al, 0.67% Zn, 0.23% Mn and Mg (bal.) by inductively coupled plasma atomic emission spectrometry (ICP-AES, Baird PS-6). The ingot AZ61 magnesium alloy was cut into 100 mm × 50 mm × 10 mm plate by high-precision wire cutting machine, and single pass rolling (10 mm to 4.5 mm) was carried out by double-roll mill. Before rolling, the sheet was heated to 400 °C in a heating furnace and kept for 30 minutes. The parameters were as follows: the reduction was 55%, the rolling temperature was 400 °C, and the rolling speed was 0.1 m s⁻¹. In order to avoid the error caused by the material size on the experimental results, the rolled and extruded AZ61 magnesium alloy were cut into 100 mm × 50 mm × 4.5 mm plates by a high-precision wire cutting machine before the electric pulse treatment. Pulse current parameters were as follows: peak current 600 A, duty cycle 50%, frequency 100 Hz, cross-sectional area 225 mm², power duration 5 minutes.

The investigated anodes were cut into block samples of 15 mm × 15 mm × 3 mm and 10 mm × 10 mm × 4.5 mm with a high-precision slow wire cutting machine (DK7625P), of which 15 mm × 15 mm × 3 mm samples were used for XRD testing, while 10 mm × 10 mm × 4.5 mm samples were used for metallographic and subsequent electrochemical tests. To ensure the accuracy of XRD test results, the oxide film on the surface of sample was polished with fine sandpaper. In addition, the samples for microstructure analysis (10 mm × 10 mm × 5 mm) were ground and polished with different SiC abrasive papers and then rusted 10 s with the corrosive mixture of 5 g picric acid, 100 mL ethanol, 5 mL acetic acid, and 10 mL distilled water.

Characterization methods

The phase constitution of the investigated anodes was examined using an X-ray diffraction meter (XRD, D/Max 2550, scan rate: 4 °C min⁻¹, and scan range: 5-80 °C). The microstructure and surface morphology of samples were observed by a JSF-6700F scanning electron microscope (SEM).

Electrochemical measurement

The electrochemical performance was measured by CHI760E electrochemical workstation. The working electrode was four kinds of magnesium alloy anode, saturated calomel electrode (SCE) and platinum plate as reference electrode and counter electrode respectively. Among them, the working area was 1 cm², the electrolyte is 3.5 wt % NaCl aqueous solutions, before electrochemical test, using different degrees of silicon carbide paper grinding working

electrode. At room temperature (25 °C) immersed in the electrolyte for 10 minutes to obtain stable open circuit potential (OCPs). The potential from -2 to -1 V (vs. SCE) was scanned at the speed of 10 mV s⁻¹, and the polarization curve was recorded. Electrochemical impedance spectroscopy (EIS) was recorded under OCPs, the voltage amplitude was 5 mV, and the frequency range was 100 kHz ~ 0.01 Hz. Then, the electrochemical impedance spectroscopy was fitted by Zsimpwin software to obtain the electrochemical parameters.

Mg-air battery analysis

Figure 1 shows a schematic diagram of an Mg-air battery. It is composed of a magnesium anode, reaction cavity, and a commercial air cathode. The working area of the anode and the cathode is 1 cm², the capacity of the reaction cavity is 12 mL, and the electrolyte is 3.5% sodium chloride solution. The cathode was the commercial air cathode for each Mg-air battery. The manufacturer (Changzhou Youteco New Energy Technology Co., Ltd.) provided air cathode. It is mainly formed by metal mesh, a waterproof breathable layer, and catalytic lamination. It is 0.6 mm thick and contains 85% MnO₂, 7.5% flake graphite and 7.5% acetylene black. The investigated magnesium alloys were used as the anodes. The specifications of all magnesium anodes were 25 mm × 70 mm × 2 mm. All investigated magnesium anodes were gradually polished with sandpaper of 800 #, 1000 #, 1200 #, 2000 # and 3000 #. After being washed with alcohol for 5 min in an ultrasonic cleaner, it was dried with cold air. An electronic balance (FA124C) with a precision of 0.1 mg was used to weigh the anodes before and after discharge. The LAND battery test system (CT2001A) was used to test the battery performance at current densities of 2.5 mA cm⁻², 5 mA cm⁻², 10 mA cm⁻² and 20 mA cm⁻². The stationary discharge period of 5 hours was recorded, and the anodic efficiency (η%) can be calculated by the following formula:

$$\eta = M_1/M_2 \times 100\%$$

$$M_1 = (i \times A \times t) / (F \times \sum(x_i \times n_i / m_i))$$

where i is the current density (mA cm⁻²), A is the surface area (cm²), t is the discharge time (h), F is the Faraday constant (96485 C mol⁻¹), x_i , n_i and m_i represent the mass fraction, ionic valence and molar mass (g mol⁻¹), respectively. Also, η , M_1 and M_2 refer to anodic efficiency (%), theoretical mass loss (g), and the actual mass loss (g), respectively. The chromic acid (200 g L⁻¹) was employed to remove the discharged products, and the discharged morphologies were observed using scanning electron microscopy.

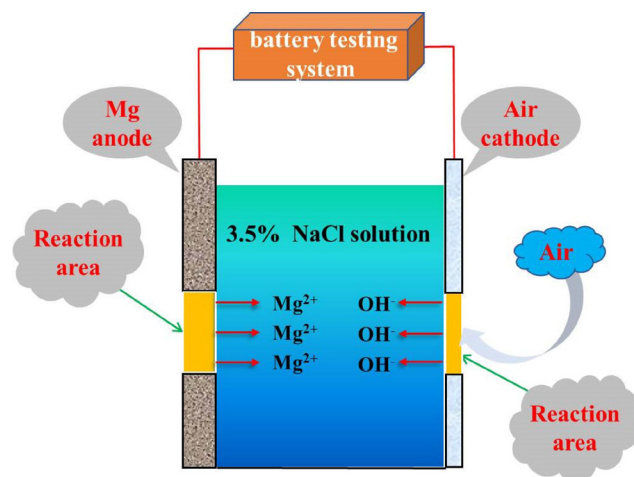


Figure 1. A schematic diagram of an Mg-air battery

RESULTS AND DISCUSSION

Microstructures

Figure 2 shows the XRD patterns of the rolled, rolled + EPT, extruded and extruded + EPT anodes. According to XRD patterns, the four magnesium anodes mainly consist of α -Mg phase (JCPDS 35-0821) and β -Mg₁₇Al₁₂ phase (JCPDS 01-1128), which is consistent with previous research results.²⁸ It is noteworthy that the diffraction peak of β -Mg₁₇Al₁₂ phase in the rolled magnesium anode after EPT is lower than that in the original rolled magnesium anode. In addition, at $2\theta = 37.5^\circ\text{C}$ and $2\theta = 48^\circ\text{C}$, the diffraction peak of α -Mg phase in the extruded magnesium alloy anode after EPT is higher than that of the original extruded magnesium alloy, indicating that electric pulse treatment can promote the dissolution of second phase in magnesium alloy. There are “thermal effect” and “non-thermal effect” in the EPT, because the “non-thermal effect” in the EPT is dominant, and on the basis of “thermal effect”, it promotes the dissolution of β -Mg₁₇Al₁₂ phase in magnesium alloy.^{29, 30}

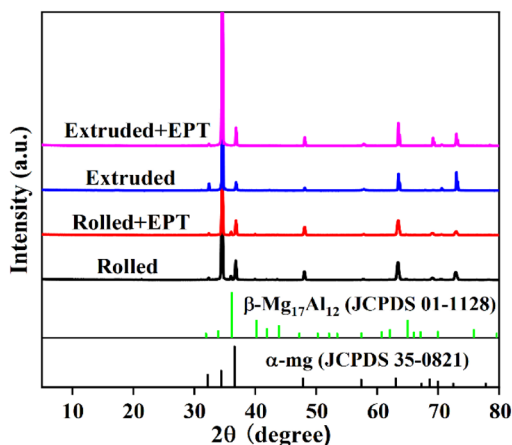


Figure 2. XRD patterns of the rolled, rolled + EPT, extruded and extruded + EPT anodes

Figure 3 shows the SEM images of the four anodes and the corresponding grain size distribution. The average grain size of rolled magnesium anode increases from 5.42 μm to 6.07 μm , and the average grain size of extruded magnesium anode increases from 29.43 μm to 32.39 μm after EPT. It indicates that the electrical pulse treatment increases the grain size. As shown in Figure 3b and 3d, the grain range of rolled magnesium anode before and after EPT is about 0-16 μm . About 87% of the grain size in the original rolled magnesium anode is between 2-8 μm , and the maximum proportion of grain size between 4-6 μm is 37.3%. About 76% of the grain size in the rolled magnesium anode after EPT is between 2-8 μm , and the maximum proportion of grain size between 4-6 μm is 33.4%. In addition, as shown in Figure 3f and 3h, the grain range of the original extruded magnesium anode is about 0-110 μm , and that of the extruded magnesium anode is about 0-70 μm after electrical pulse treatment. In the original rolled magnesium anode, about 88% of the grain size is between 10-50 μm , and the maximum proportion of grain size between 20-30 μm is 35.8%. However, about 87% of the grain size of extruded magnesium anode after EPT is between 10-50 μm , and the maximum proportion of grain size between 20-30 μm is 28.4%. This means that the microstructure of magnesium anode after EPT is more uniform.

Polarization curves

Figure 4 shows the polarization curves of the investigated

anodes in 3.5% NaCl solution, and electrochemical parameters are summarized in Table 1. As shown in Figure 4, the cathodic polarization curves of the four anodes are basically similar, but the anodic polarization curves are different. It is well known that the dissolution of magnesium alloy is closely related to the anodic polarization curve, and the cathodic polarization curve is mainly attributed to the hydrogen evolution reduction reaction on the surface of magnesium alloy.³¹ In addition, self-passivation can be observed in the branches of the rolled anode and the rolled anode after EPT, which means that the formed anode film (magnesium oxide and magnesium hydroxide corrosion product film) acts as a physical shield to further prevent the anode self-discharge.³² Four research anodes have different passivation positions, which is the root cause of the difference in discharge behavior. As shown in Table 1, the order of four anodic corrosion potentials from negative to positive is: Extruded + EPT < Extruded < Rolled + EPT < Rolled. In the discharge process as an anode, the anode with more negative corrosion potential reacts more positively to the current, which means it has higher electrochemical activity.³³ The corrosion potential of both rolled and extruded anodes shifted negatively after EPT, indicating that EPT can effectively improve the electrochemical activity of magnesium anode. It is worth noting that the difference in the corrosion potential of the rolled anode before and after EPT is 42 mV, while that of the extruded anode is only 24 mV. Therefore, it can be concluded that the effect of the rolled anode treated by electric pulse is better than that of the extruded anode. Studies have shown that different dislocation densities in the alloy lead to different dissolution rates of β -Mg₁₇Al₁₂ during electric pulse treatment, and ultimately affect the volume fraction of the second phase in the alloy.³⁴ This is the fundamental reason for the difference of the electrochemical performance between the rolled and extruded anodes by EPT.

Electrochemical impedance spectra (EIS)

Figure 5 shows the electrochemical impedance spectra (EIS) in Nyquist and Bode plots of the rolled, rolled + EPT, extruded and extruded + EPT anodes at OCPs. As shown in Figure 5a, the Nyquist plots of the four anodes are composed of two semicircles of high and low frequency, indicating that their corrosion mechanisms are similar. Due to different diameters, the final electrochemical activities are different. The semicircle in the high frequency region is a capacitive arc, which is mainly related to the double layer capacitance and charge transfer resistance.³⁵ Studies have shown that the charge transfer resistance is negatively correlated with the corrosion rate of magnesium alloy anodes, that is, magnesium alloy anodes with small charge transfer resistance will show a higher corrosion rate and are more likely to be activated and dissolved in electrolyte at corresponding test potential.³⁶ The low-frequency semicircle in the fourth quadrant is the inductive arc, representing the desorption of the anodic surface products. In addition, the low frequency induced reactance arc is caused by the chemical reaction between Mg²⁺ and water and the desorption of corrosion products.³⁷ As shown in the bode diagram of Figure 5b, the impedance modulus values of the four anodes are arranged in descending order as: Extruded + EPT < Extruded < Rolled + EPT < Rolled. The lower impedance modulus indicates that magnesium anode is easier to dissolve during discharge.³⁸ This indicates that EPT can improve the corrosion rate of magnesium anode, which is consistent with the polarization curve test results.

In order to further study the corrosion process of magnesium anode, the equivalent circuit diagrams of the four anodes are shown in Figure 5c, where R_s and R_T represent the solution resistance and charge transfer resistance, respectively. Due to the deviation between

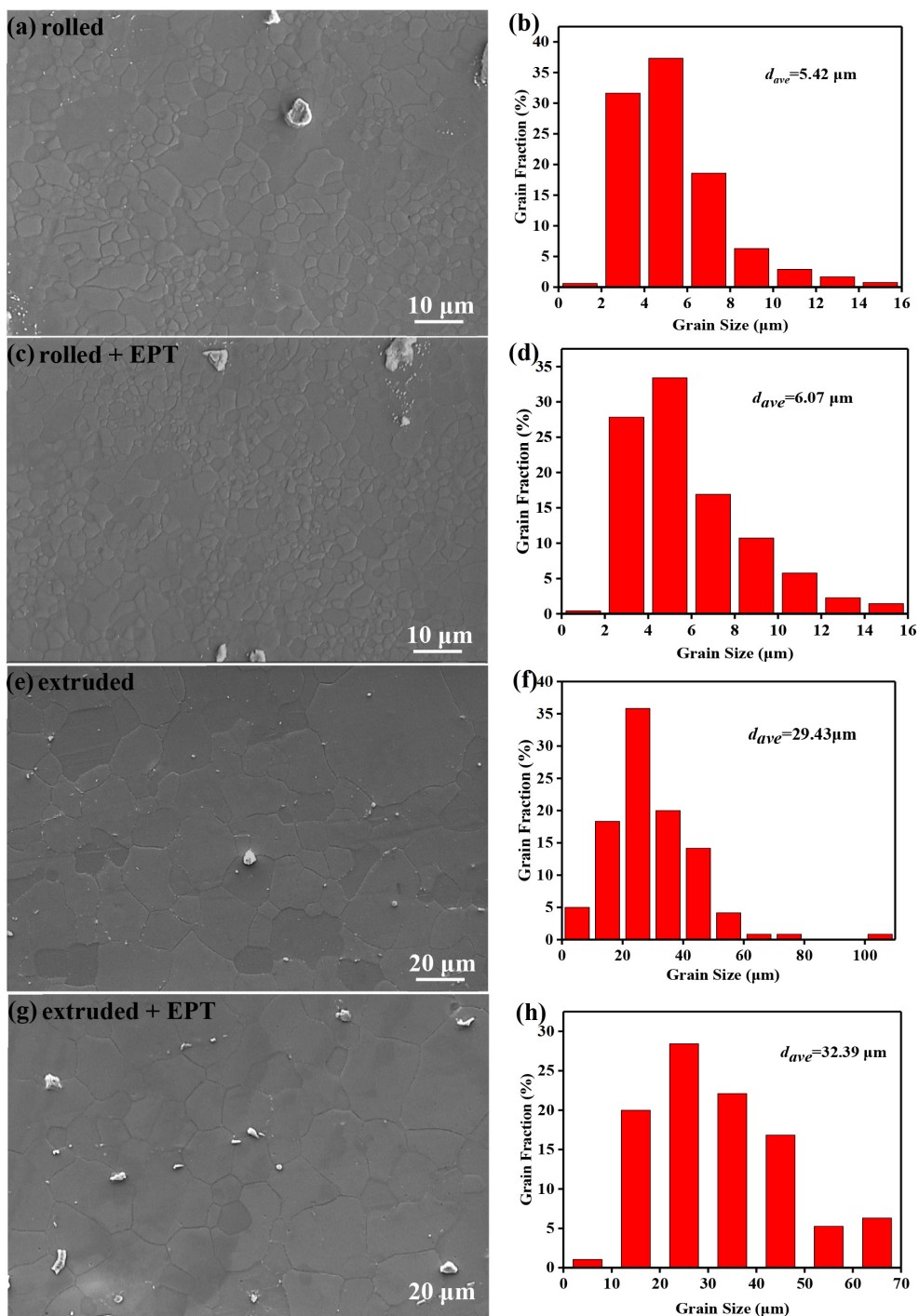


Figure 3. The SEM images of the four anodes and the corresponding grain size distribution: (a) and (b) rolled, (c) and (d) rolled + EPT, (e) and (f) extruded, (g) and (h) extruded + EPT

the actual capacitance of the double electric layer and the standard capacitance, Q represents the capacitance of the double electric layer at the electrode / electrolyte interface. The inductive reactance in the low-frequency region is characterized by R_L and L series, which is caused by the desorption of corrosion products.³⁹

Table 2 shows the fitting results based on equivalent circuits. The impedance modes of the four anodes are arranged in descending order as follows: Extruded + EPT ($1306.7 \Omega \text{ cm}^2$) < Extruded ($1408.9 \Omega \text{ cm}^2$) < Rolled + EPT ($1764.81 \Omega \text{ cm}^2$) < Rolled ($2244.10 \Omega \text{ cm}^2$). Generally, lower R_T implies higher activity,⁴⁰ proportional to the anodic dissolution rate. It should be noted that the impedance modulus of the rolled anode decreased from $2244.10 \Omega \text{ cm}^2$

to $1764.81 \Omega \text{ cm}^2$ with a difference of 479.29, while the impedance modulus of the extruded anode decreased from $1408.9 \Omega \text{ cm}^2$ to $1306.7 \Omega \text{ cm}^2$ with a difference of 102.1. The test results are in good agreement with the polarization curve, which proves once again that the effect of the rolled anode treated by electric pulse is better than that of the extruded anode. In addition, the Q value of magnesium anode reflects the difficulty of forming dense oxide film on its surface, that is, the lower the Q value is, the easier it is to form dense oxide film on the anode surface.⁴¹ The Q values of the rolled anode are larger than those of the extruded anode, which means that loose oxide film is formed on the surface of the rolled anode, which is conducive to the stripping of corrosion products and thus improves the efficiency

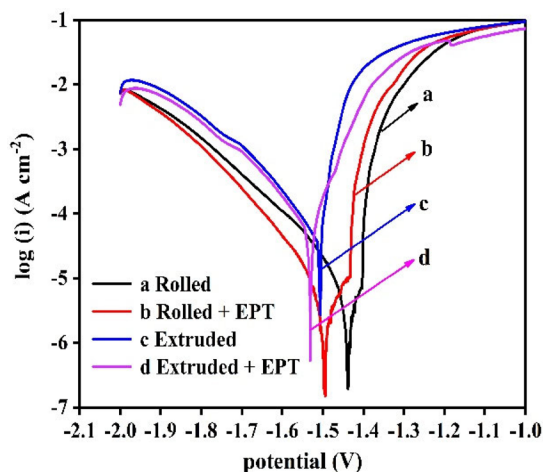


Figure 4. Polarization curves of the investigated anodes in 3.5% NaCl solution

Table 1. Electrochemical parameters of different anodes

Magnesium anode	E_{corr} (vs. SCE) / V	J_{corr} / (A cm^{-2})
Rolled	-1.454	1.680×10^{-5}
Rolled + EPT	-1.496	6.702×10^{-5}
Extruded	-1.507	7.887×10^{-5}
Extruded + EPT	-1.531	11.662×10^{-5}

of the anode. Studies have shown that a small R_L value means that the corrosion products are porous, which facilitates the contact between the magnesium anode and electrolyte, thereby enhancing the discharge performance.⁴² Therefore, during the discharge process, the magnesium anode with lower R_T value has a faster dissolution rate in the electrolyte and higher discharge activity. In addition, the corrosion products on the surface of the magnesium anode with a small R_L value are easy to fall off, thereby increasing the anode discharge activity.

Mg-air batteries performance

Figure 6 displays the voltage-time curves of batteries using investigated alloys as anodes at different current densities (2.5 mA cm^{-2} , 5 mA cm^{-2} , 10 mA cm^{-2} and 20 mA cm^{-2}). Table 3 shows the average discharge battery voltage of the anode and the voltage difference before and after EPT. With the increase of current density, the average battery voltage of the four anodes decreased continuously. This phenomenon was attributed to the discharge products formed during the discharge process, which hindered the direct contact between the fresh magnesium matrix and the electrolyte. In the early stage of discharge, the voltage drops very quickly. The reason is that at the beginning of the discharge behavior, the alloy surface morphology changes rapidly, and the discharge product shedding rate is lower than the generation rate, which reduces the discharge voltage.⁴³ With the passage of discharge time, the formation and shedding of discharge products reach dynamic equilibrium. The average battery voltage of the magnesium anode treated by electric pulse is higher than that of the original rolled or extruded anode. It can be concluded that EPT can improve the discharge voltage of magnesium alloy. This is because EPT can increase the grain size of magnesium anode. Studies show that the discharge performance is related to the type of material, the number of twins, grain size and grain uniformity. Large grain size means higher discharge activity.^{44,45}

When the discharge density is 2.5 mA cm^{-2} , the average battery voltage of the rolled anode is 1.2853 V and 1.3116 V, respectively, with a difference of 53.3 mV. The average cell voltage of the extruded

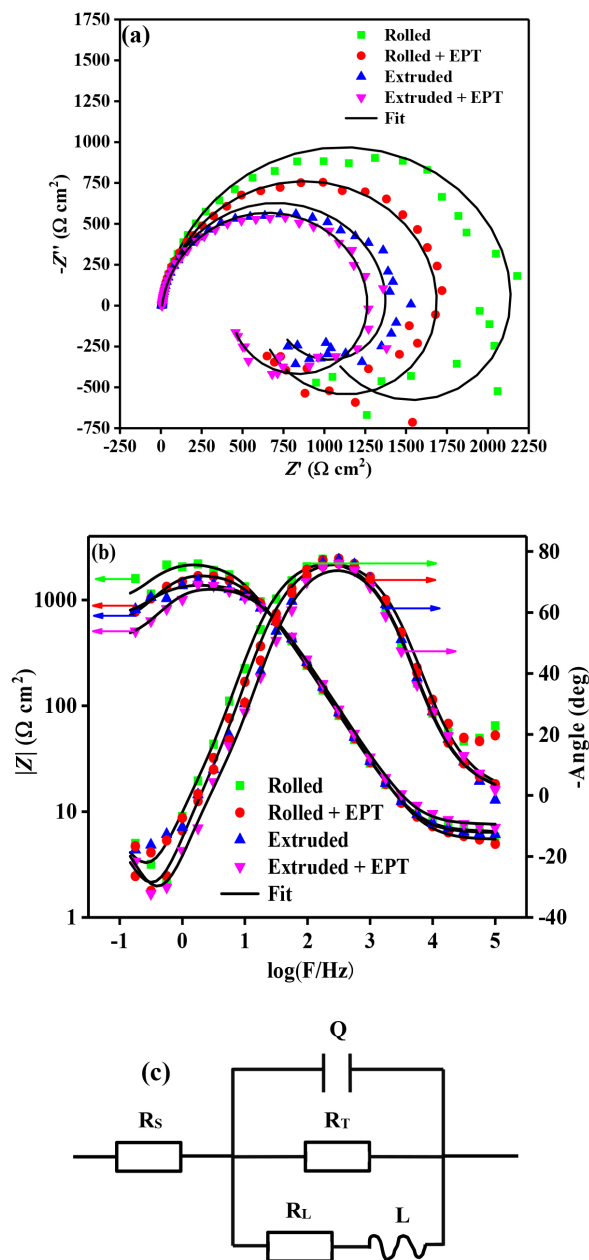


Figure 5. Electrochemical impedance spectra of the rolled, rolled + EPT, extruded and extruded + EPT anodes in 3.5 wt. % NaCl solution: (a) Nyquist plots, (b) Bode plots and (c) Equivalent circuit of different anodes

anode is 1.2993 V and 1.2998 V, respectively, with a difference of 0.5 mV. It is worth noting that under all test discharge densities, the voltage difference of the rolled anode before and after electrical pulse treatment is far greater than that of the extruded anode, which means that the effect of the rolled anode after electrical pulse treatment is better than that of the extruded anode.

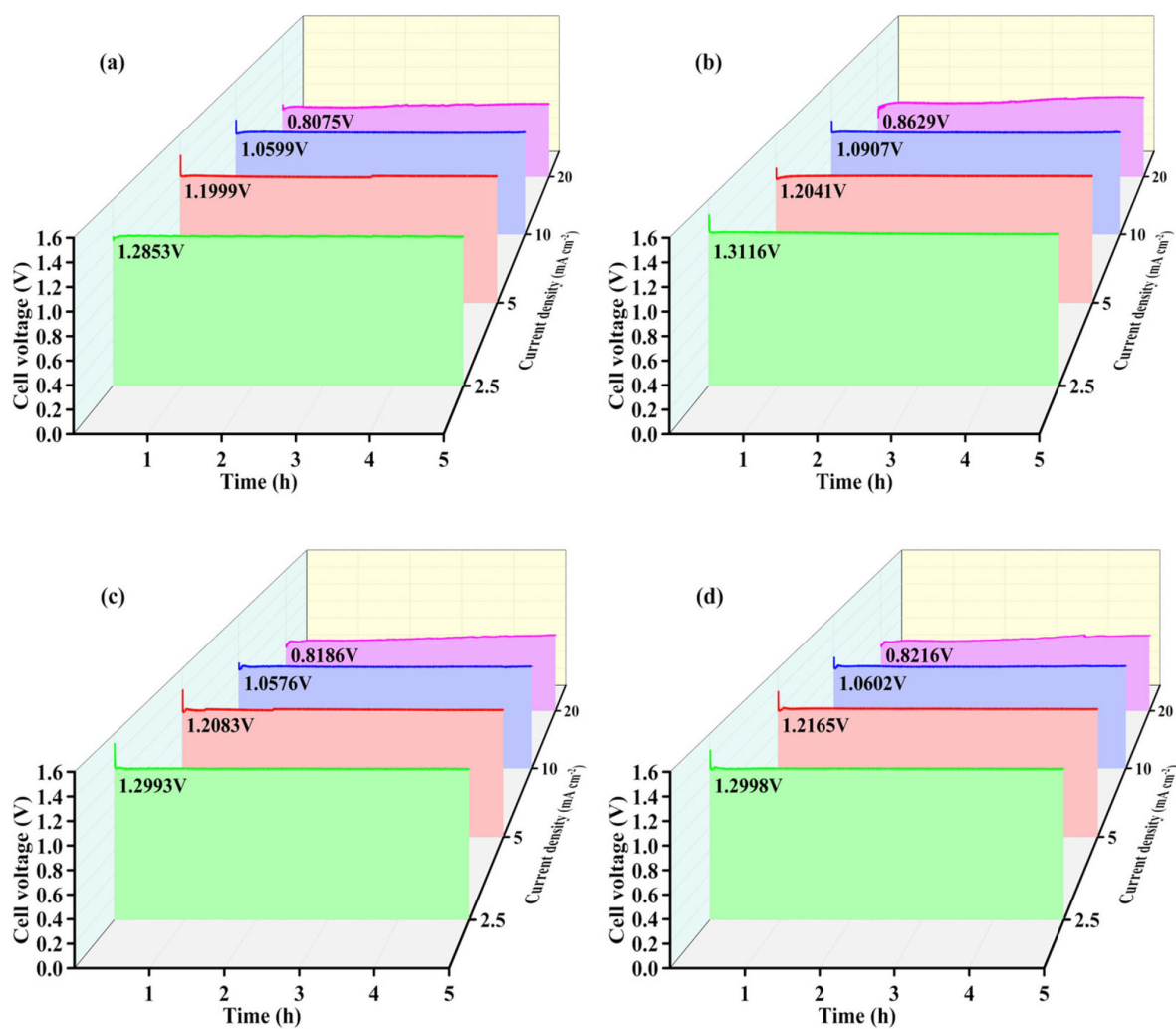
In addition, it can be obviously observed that the discharge curve of the magnesium anode without electrical pulse treatment has an upward inflection point, which should be the time point for the discharge product to fall off. It reflects from the side that the generation rate of the discharge product of the anode is greater than the falling rate, while there is almost no inflection point for the magnesium anode after EPT, which is particularly obvious when the discharge density is 5 mA cm^{-2} .

Throughout the discharge process, the magnesium anode (rolled and extruded) treated with electric pulse consistently had higher

Table 2. Summarizes the fitting values of impedance parameters obtained by Zsimpwin software according equivalent circuit

Magnesium anode	$R_s / \Omega \text{ cm}^2$	$Q / \Omega^{-1} \text{ cm}^2 \text{ s}^n$	n	$R_T / \Omega \text{ cm}^2$	$L / \Omega \text{ cm}^2 \text{ s}$	$R_L / \Omega \text{ cm}^2$
Rolled	6.45	1.21×10^{-5}	0.91	2244.10	1404.3	1667.7
Rolled + EPT	5.42	1.17×10^{-5}	0.90	1764.81	713.7	888.7
Extruded	6.30	1.01×10^{-5}	0.93	1408.9	989.6	1370.5
Extruded + EPT	7.54	1.03×10^{-5}	0.91	1306.7	410.5	600.7

R_s : the solution resistance; Q : the interface capacitance of the double electric layer; n : the equivalent to the dispersion factor; R_T : the charge transfer resistance; L : inductance; R_L : inductance resistance.

**Figure 6.** Discharge curves of assembled Mg-air batteries: (a) Rolled, (b) Rolled + EPT, (c) Extruded and (d) Extruded+ EPT**Table 3.** Average discharge potentials of different anodes obtained from the potential-time curves at different current densities

Magnesium anode	Current Density (mA cm ⁻²)	Average discharge potential (V, vs. SCE)		Voltage difference (mV)
		Without EPT	EPT	
Rolled	2.5	1.2583	1.3116	53.3
	5	1.1199	1.2041	84.2
	10	1.0599	1.0907	30.8
	20	0.8075	0.8629	55.4
Extruded	2.5	1.2993	1.2998	0.5
	5	1.2083	1.2165	8.2
	10	1.0576	1.0602	2.6
	20	0.8186	0.8216	3

and stable battery voltage, which may be partly attributed to the existence of micro-cracks on the discharge surface, as shown in Figure 7. When the discharge density is 20 mA cm⁻², the discharge curves of the four magnesium anodes are extremely unstable, which is because the discharge products are easier to form at high current density, and the current density slows down the accumulation of corrosion product films, leading to the unstable operating voltage in the discharge process.⁴⁶

Table 4 shows the discharge parameters of the Mg-air cells using the studied alloy as anode under various current densities. The discharge capacity and anode efficiency increase with the increase of current density. It was obvious that the discharge activity of magnesium anode was significantly improved by electric pulse treatment. At the same current density, the anode efficiency, discharge capacity and specific energy of the magnesium anode after electrical pulse treatment are higher than those of the original anode. Combined with Figure 6 and Table 3, the results show that the magnesium anode treated by electric pulse has excellent discharge performance and stable discharge curve. This phenomenon may be attributed to the following two conclusions: (1) the β -Mg₁₇Al₁₂ phase in magnesium anode is dissolved by electric pulse treatment due to the presence of non-thermal effect. Studies have shown that the coarse β -Mg₁₇Al₁₂ particles can accelerate the hydrogen evolution reaction of magnesium anode, resulting in serious self-corrosion, resulting in very poor anode efficiency and specific energy.^{47,48} Because β -Mg₁₇Al₁₂ phase is more in the original magnesium anode (rolled and extruded), the discharge performance of the original magnesium anode is lower than that of the magnesium anode treated by electric pulse; (2) EPT can make the grains more uniform. It can promote the magnesium matrix to react evenly with the electrolyte during the discharge process, thus obtaining a stable discharge curve.⁴⁹ It is worth noting that compared with the extruded magnesium anode, the effect of EPT on the rolled magnesium anode is more obvious, especially at the discharge density of 5 mA cm⁻². This is due to the different dislocation densities in the rolled and extruded magnesium anode. In the process of electric pulse processing, the different dislocation densities in the alloy will lead to different dissolution rates of β -Mg₁₇Al₁₂, and ultimately affect the volume fraction of the second phase in the alloy.³⁴ In addition, there

are many factors that affect the effect of EPT, such as frequency, duty cycle, current and material itself.^{50,51} In this work, the same pulse parameters are used. Compared with the rolling state, the complex internal structure of the extruded state a larger pulse current. Therefore, it can be inferred that EPT can greatly improve the discharge performance of the rolled magnesium anode.

Surface morphologies after the discharge

Figure 7 shows the surface morphologies of the investigated anodes after removing the discharge products at a current density of 5 mA cm⁻² for 5 h. The surface morphology of the four anodes is different, which is the fundamental reason for the difference of discharge behavior. Figure 7a shows that a local reaction occurs on the surface of the rolled magnesium anode, forming some pits, which means that the anode undergoes a block effect of metal particles.⁵² It results in additional mass loss and thus reduces the anode efficiency. As shown in Figure 7c, the surface of the extruded magnesium anode is coral-like. During the discharge process, this structure will become the porous container for the discharge product Mg(OH)₂, which will hinder the contact between the Mg matrix and sodium chloride solution, resulting in unstable discharge and low efficiency.⁵³ As shown in Figure 7b and 7d, after EPT, the discharge pits on the surface of the rolled and extruded anode are shallower and less, and the surface is smoother, which is conducive to the shedding of discharge products on the anode surface, thus providing stable battery voltage.⁵⁴ In addition, micro-cracks are formed on the discharge surface of the rolled and extruded anodes after EPT, indicating that the discharge products were easy to peel off from the surface of the alloy, which increased the contact area between magnesium anode and NaCl solution, thus improving the discharge performance.⁵⁵ The results confirm the hypothesis that electric pulse treatment can improve the discharge performance of magnesium anode. It is noteworthy that there are more micro-cracks on the surface of the rolled anode and in the discharge pit after EPT (Figure 7b), while there are a few micro-cracks on the surface of the extruded magnesium anode after EPT, which fundamentally explains the significant effect of electric pulse treatment on the rolled anode.

Table 4. Discharge parameters of Mg-air batteries with different anode under various current densities

Current Density (mA cm ⁻²)	Magnesium anode	Anode efficiency (%)	Capacity density (mAh g ⁻¹)	Energy density (mWh g ⁻¹)
2.5	Rolled	51.346 ± 0.625	1149.721 ± 2.980	1507.974 ± 3.014
	Rolled + EPT	52.971 ± 0.124	1186.053 ± 5.581	1524.434 ± 7.171
	Extruded	50.153 ± 0.574	1122.959 ± 5.459	1459.622 ± 5.898
	Extruded + EPT	51.573 ± 0.341	1154.753 ± 3.186	1500.371 ± 4.141
5	Rolled	54.923 ± 0.441	1229.752 ± 4.587	1480.744 ± 5.524
	Rolled + EPT	56.389 ± 0.365	1262.596 ± 7.868	1514.989 ± 9.439
	Extruded	52.165 ± 0.298	1167.998 ± 6.301	1420.869 ± 7.667
	Extruded + EPT	53.419 ± 0.507	1196.099 ± 4.471	1445.247 ± 5.402
10	Rolled	59.033 ± 0.602	1321.779 ± 6.521	1402.011 ± 7.916
	Rolled + EPT	60.131 ± 0.271	1346.359 ± 9.691	1427.006 ± 8.274
	Extruded	55.904 ± 0.304	1251.719 ± 8.602	1327.073 ± 6.231
	Extruded + EPT	57.112 ± 0.568	1278.772 ± 5.961	1352.429 ± 4.635
20	Rolled	62.464 ± 0.847	1398.601 ± 7.502	1206.853 ± 6.536
	Rolled + EPT	63.082 ± 0.107	1412.429 ± 8.791	1140.537 ± 3.561
	Extruded	57.479 ± 0.247	1287.001 ± 6.309	1053.539 ± 3.984
	Extruded + EPT	58.765 ± 0.407	1315.789 ± 6.541	1081.053 ± 4.356

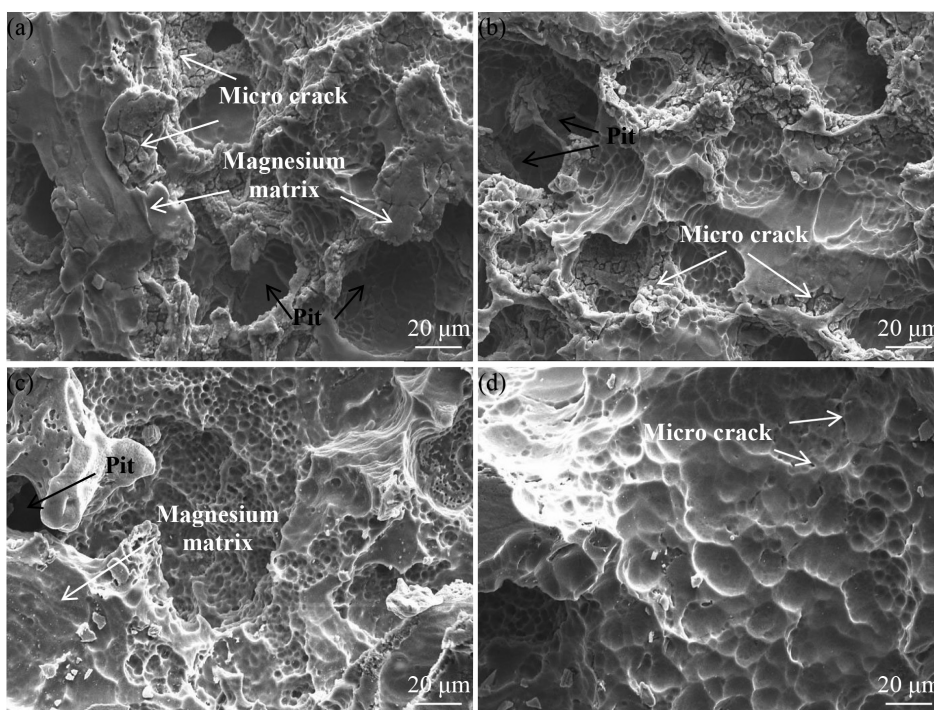


Figure 7. SEM images of surface morphologies for the investigated anodes in 3.5 wt.% NaCl solution after removing the discharge products. (a) Rolled, (b) Rolled + EPT, (c) Extruded and (d) Extruded+ EPT

CONCLUSIONS

In this work, rolled and extruded AZ61 magnesium alloy was used as the anode of Mg-air battery. Meanwhile, the magnesium anode was characterized by SEM and XRD, and the effects of electric pulse treatment on its microstructure, corrosion behavior, electrochemical performance and battery performance were studied. The results show that electric pulse treatment has a positive effect on the electrochemical performance and discharge performance of magnesium anode. Compared with the original magnesium anode, the magnesium anode treated by electric pulse showed higher electrochemical activity, stable discharge curve, excellent specific energy and higher anode efficiency. The reason is that electric pulse treatment can make the coarse second phase in magnesium anode dissolve and the grains become more uniform. In addition, micro-cracks can be formed on the surface of magnesium anode after electric pulse treatment, which is beneficial to promote the self-stripping of discharge products and improve the discharge performance. In particular, the effect of the rolled anode treated by electric pulse is better than that of the extruded anode. It may be because of the different dislocation density in the two magnesium alloys. During the electric pulse treatment, the dislocation density in the alloy is highly correlated with the dissolution rate of β -Mg₁₇Al₁₂, which ultimately affects the volume fraction of the second phase in the alloy. In conclusion, electro pulse treatment can greatly improve the electrochemical and discharge properties of magnesium alloy anode, which is very suitable for the preparation of magnesium alloy anode sheet.

ACKNOWLEDGEMENTS

This project was funded by the major science and technology projects of Shanxi Province (20201102003), Project supported by national key R & D program 2018YFB1308701, the National Natural Science Foundation of China (52075357), the National Key Research and Development Plan (2018YFA0707301), and project supported by the open fund of State Key Laboratory of high-performance

complex manufacturing, Central South University (Kfkt2019-03), The Graduate Education Innovation Project of Shanxi Province (2021Y672 and 2021Y687).

REFERENCES

- Wang, H. F.; Qiang, X.; *Mater* **2019**, *1*, 565. [Crossref]
- Rahman, M. A.; Wang, X.; Wen, C.; *J. Electrochem. Soc.* **2013**, *160*, 1759. [Crossref]
- Wu, Y. P.; Wang, Z. F.; Liu, Y.; Li, G. F.; Xie, S. H.; Yu, H.; Xiong, H. Q.; *J. Mater. Eng. Perform.* **2019**, *28*, 2006-2016. [Crossref]
- Xu, C.; Nakata, T.; Fan, G. H.; Li, X. W.; Tang, G. Z.; Kamado, S.; *J. Magnesium Alloys* **2019**, *7*, 388. [Crossref]
- Shrestha, N.; Raja, K. S.; Utgikar, V.; *J. Electrochem. Soc.* **2019**, *166*, 3139. [Crossref]
- Feng, Y.; Xiong, W. H.; Zhang, J. C.; Wang, R. C.; Wang, N. G.; *J. Mater. Chem. A* **2016**, *4*, 8658. [Crossref]
- Wang, N. G.; Li, W. P.; Huang, Y. X.; Wu, G.; Hu, M. C.; Li, G. Z.; Shi, Z. C.; *J. Power Sources* **2019**, *436*, 226855. [Crossref]
- Liu X.; Xue, J. L.; Zhang, P. J.; Wang, Z. J.; *J. Power Sources* **2019**, *414*, 174. [Crossref]
- Chen, X. R.; Ning, S. C.; Le, Q. C.; Wang, H. N.; Zou, Q.; Guo, R. Z.; Hou, J.; Jia, Y. H.; Atrens, A.; Yu, F. X.; *J. Mater. Sci. Technol. (Shenyang, China)* **2020**, *38*, 47. [Crossref]
- Shi, Y. C.; Peng, C. Q.; Feng, Y.; Wang, R. C.; Wang, N. G.; *Mater. Des.* **2017**, *124*, 24. [Crossref]
- Li, J. R.; Jiang, Q. T.; Sun, H. Y.; Li, Y. T.; *Corros. Sci.* **2016**, *111*, 288. [Crossref]
- Li, L.; Wang, T.; Wang, Y.; Zhang, C. C.; Lv, H.; Lin, H.; Yu, W. B.; Huang, C. J.; *J. Magnesium Alloys* **2020**, *8*, 499. [Crossref]
- Chen, X. R.; Wang, H. N.; Zou, Q.; Le, Q. C.; Wen, C.; Atrens, A.; *Electrochim. Acta* **2021**, *367*, 137518. [Crossref]
- Cao, F. Y.; Zhang, J.; Li, K. K.; Song, G. L.; *Trans. Nonferrous Met. Soc. China* **2021**, *31*, 939. [Crossref]
- Li, Z.; Peng, Z. Y.; Qiu, Y. B.; Qi, K.; Chen, Z. Y.; Guo, X. P.; *J. Mater. Res. Technol.* **2020**, *9*, 11201. [Crossref]

16. Ma, Y. L.; Xiong, H. W.; Chen, B. Y.; *Corros. Sci.* **2021**, *191*, 109759. [Crossref]
17. Wang, X. W.; Wang, W.; Chen, W.; Chen, D. M.; *J. Mater. Sci. Technol. (Shenyang, China)* **2022**, *98*, 219. [Crossref]
18. Jana, A.; Das, M.; Balla, V. K.; *J. Alloys Compd.* **2020**, *821*, 153462. [Crossref]
19. Kim, M. J.; Lee, M. G.; Hariharan, K.; Hong, S. T.; Choi, I. S.; Kim, D.; Oh, K. H.; Han, H. N.; *Int. J. Plast.* **2017**, *94*, 148. [Crossref]
20. Jiang, Y. B.; Tang, G. Y.; Shek, C. H.; Liu, W.; *J. Alloys Compd.* **2011**, *509*, 4308. [Crossref]
21. Yang, H. B.; Wu, L.; Jiang, B.; Liu, W. J.; Xie, H. M.; Song, J. F.; Huang, G. S.; Zhang, D. F.; Pan, F. S.; *J. Electrochem. Soc.* **2020**, *167*, 121503. [Crossref]
22. Li, Q.; Xiong, W.; Yu, M. H.; Li, J.; Liu, L.; Zhu, G.; Wang, L. Y.; Wang, J.; Yu, S. R.; Liu, E. Y.; *J. Alloys Compd.* **2022**, *891*, 161914. [Crossref]
23. Huang, K.; Cayron, C.; Logé, R. E.; *Mater. Charact.* **2017**, *129*, 121. [Crossref]
24. Liu, K.; Dong, X. H.; Xie, H. Y.; Wu, Y. J.; Fang, P.; *J. Alloys Compd.* **2016**, *676*, 106. [Crossref]
25. Liu, Y.; Fan, J. F.; Zhang, H.; Jin, W.; Dong, H. B.; Xu, B. S.; *J. Alloys Compd.* **2015**, *622*, 229. [Crossref]
26. Chen, L.; Li, S. S.; Chu, X. R.; Zhao, G. Q.; Gao, J.; *Mater. Lett.* **2019**, *241*, 104. [Crossref]
27. Xiao, H.; Zhang, K. F.; Shi, C. C.; Lu, Z.; Jiang, J. F.; *J. Alloys Compd.* **2019**, *784*, 1234. [Crossref]
28. Chen, H.; Tang, J. W.; Gong, W. W.; Gao, Y. P.; Tian, F.; Chen, L.; *J. Mater. Res. Technol.* **2021**, *15*, 4800. [Crossref]
29. Jeong, H. J.; Kim, M. J.; Park, J. W.; Yim, C. D.; Kim, J. J.; Oh, D. K.; Madakashira, P. P.; Han, H. N.; *Mater. Sci. Eng., A* **2017**, *684*, 668. [Crossref]
30. Jiang, Y. B.; Tang, G. Y.; Shek, C. H.; Zhu, Y. H.; Xu, Z. H.; *Acta Mater.* **2009**, *57*, 4797. [Crossref]
31. Tong, F. L.; Chen, X. Z.; Wang, Q.; Wei, S. H.; Gao, W.; *J. Alloys Compd.* **2021**, *857*, 157579. [Crossref]
32. Yuasa, M.; Huang, X. S.; Suzuki, K.; Mabuchi, M.; Chino, Y.; *J. Power Sources* **2015**, *297*, 449. [Crossref]
33. Medhashree, H. A.; Shetty, N.; *J. Mater. Res. Technol.* **2017**, *6*, 40. [Crossref]
34. Moustafa, E. T.; Kristián, M.; Gerardo, G.; Tsubasa, M.; Michiaki, Y.; Yoshihito, K.; Jenő, G.; *J. Alloys Compd.* **2019**, *771*, 629. [Crossref]
35. Xiao, B.; Song, G. L.; Zheng, D. J.; Cao, F. Y.; *Mater. Des.* **2020**, *194*, 108931. [Crossref]
36. Wang, N. G.; Wang, R. C.; Feng, Y.; Xiong, W. H.; Zhang, J. C.; Deng, M.; *Corros. Sci.* **2016**, *112*, 13. [Crossref]
37. Ma, J. L.; Zhang, Y.; Ma, M. S.; Qin, C. H.; Ren, F. Z.; Wang, G. X.; *Corros. Sci.* **2020**, *170*, 108695. [Crossref]
38. Zhao, Y. C.; Huang, G. S.; Zhang, C.; Peng, C.; Pan, F. S.; *Mater. Chem. Phys.* **2018**, *218*, 256. [Crossref]
39. Liu, X.; Xue, J. L.; Liu, S. Z.; *Mater. Des.* **2018**, *160*, 138. [Crossref]
40. Cheng, S. M.; Cheng, W. L.; Gu, X. J.; Yu, H.; Wang, Z. F.; Wang, H. X.; Wang, L. F.; *J. Alloys Compd.* **2020**, *823*, 153779. [Crossref]
41. Pokharel, D. B.; Wu, L. P.; Dong, J. H.; Yadav, A. P.; Subedi, D. B.; Dhakal, M.; Zha, L.; Mu, X.; Umoh, A. J.; Ke, W.; *J. Mater. Sci. Technol. (Shenyang, China)* **2021**, *81*, 97. [Crossref]
42. Wu, J. L.; Wang, R. C.; Feng, Y.; Peng, C. Q.; *J. Alloys Compd.* **2018**, *765*, 736. [Crossref]
43. Feng, Y.; Lei, G.; He, Y. Q.; Wang, R. C.; Wang, X. F.; *Trans. Nonferrous Met. Soc. China* **2018**, *28*, 2274. [Crossref]
44. Wang, N. G.; Huang, Y. X.; Liu, J. J.; Yang, X. S.; Xie, W. P.; Cai, Q.; Zheng, S. Y.; Shi, Z. C.; *Electrochim. Acta* **2021**, *378*, 138135. [Crossref]
45. Yang, H. B.; Wu, L.; Jiang, B.; Liu, W. J.; Song, J. F.; Huang, G. S.; Zhang, D. F.; Pan, F. S.; *J. Mater. Sci. Technol. (Shenyang, China)* **2021**, *62*, 128. [Crossref]
46. Wen, L.; Yu, K.; Xiong, H. Q.; Dai, Y. L.; Yang, S. H.; Qiao, X. Y.; Teng, F.; Fan, S. F.; *Electrochim. Acta* **2016**, *194*, 40. [Crossref]
47. Ma, J. L.; Wang, G. X.; Li, Y. Q.; Ren, F. Z.; Alex, A.; *Ionics* **2019**, *25*, 2201. [Crossref]
48. Song, Y. F.; Ma, J. L.; Li, Y. Q.; Wang, G. X.; Qin, C. H.; Stock, H. R.; *Ionics* **2019**, *25*, 5899. [Crossref]
49. Li, Z. Y.; Wang, H. X.; Li, J. J.; Zhuang, Y. P.; Gao, J. Z.; Li, H.; Cheng, W. L.; *Adv. Eng. Mater.* **2020**, *22*, 1901332. [Crossref]
50. Zhou, Q.; Chen, L. P.; Yin, J.; *Advanced Materials Research* **2012**, *399*, 1613. [Crossref]
51. Kuang, J.; Du, X. P.; Al-Samman, T.; Li, X. H.; Liu, G.; Sun, J.; *Metall. Mater. Trans. A* **2020**, *51*, 6640. [Crossref]
52. Wang, N. G.; Wang, R. C.; Peng, C. Q.; Feng, Y.; *Corros. Sci.* **2014**, *81*, 85. [Crossref]
53. Zou, Q.; Le, Q. C.; Chen, X. R.; Jia, Y. H.; Ban, C. Y.; Wang, T.; Wang, H. N.; Guo, R. Z.; Ren, L.; Atrens, A.; *Electrochim. Acta* **2022**, *401*, 139372. [Crossref]
54. Liu, X.; Xue, J. L.; Zhang, D.; *J. Alloys Compd.* **2019**, *790*, 822. [Crossref]
55. Liu, H.; Yan, Y.; Wu, X. H.; Fang, H. J.; Chu, X.; Huang, J. F.; Zhang, J. X.; Song, J. M.; Yu, K.; *J. Alloys Compd.* **2021**, *859*, 157755. [Crossref]